Experiments in Fluids (2021) 62:205
https://doi.org/10.1007/s00348-021-03301-9

RESEARCH ARTICLE

Synchronous vortex shedding from aerodynamically isolated side-by-side cylinders imposed by flow-excited resonant acoustic modes

Mahmoud Shaaban[1] · **Atef Mohany**[1]

Received: 11 May 2021 / Revised: 2 September 2021 / Accepted: 3 September 2021
© The Author(s), under exclusive licence to Springer-Verlag GmbH Germany, part of Springer Nature 2021

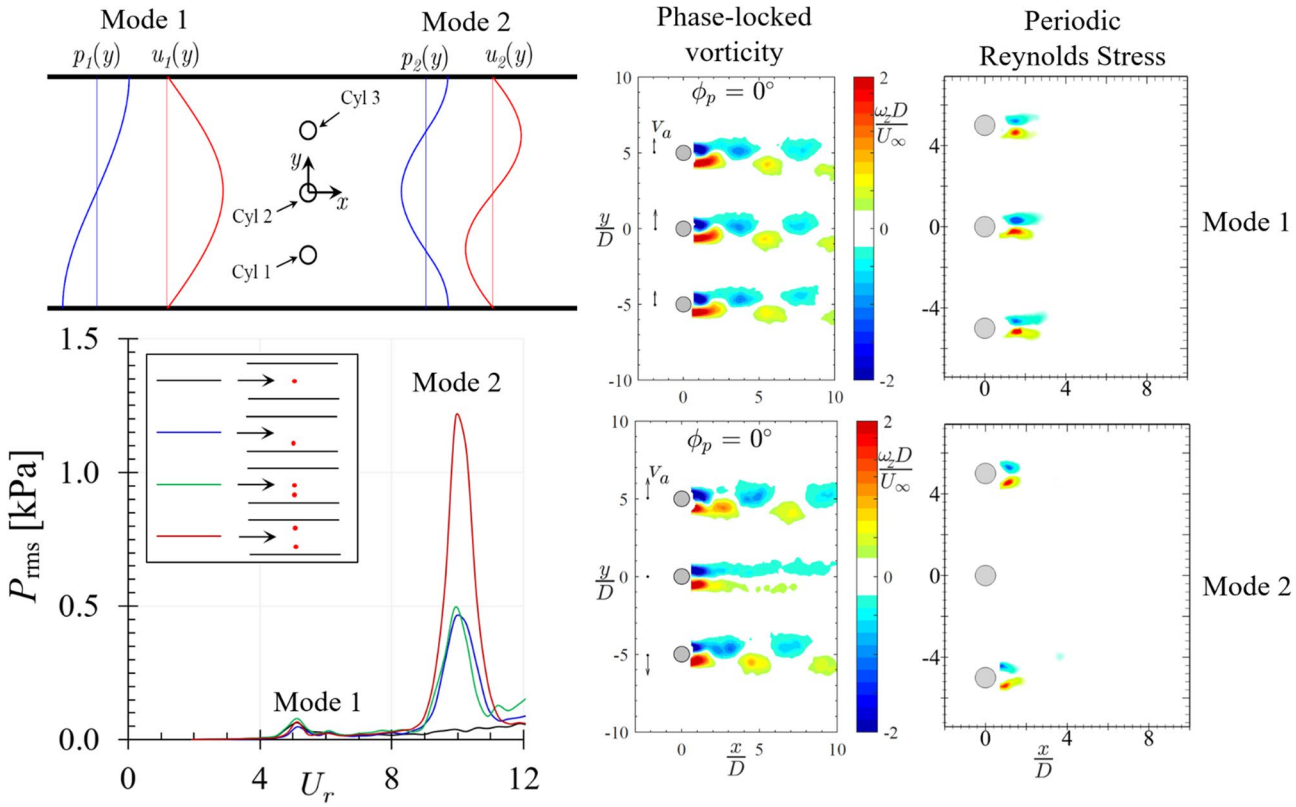
Abstract
The flow-excited acoustic resonance of aerodynamically isolated side-by-side cylinders is experimentally investigated to identify the influence of the resonant acoustic field on the dynamics of vortex shedding in the wake of the cylinders. Self-excitation of the acoustic cross-modes inside the duct housing the cylinders is achieved when the vortex shedding from the cylinders occurs at locations away from the acoustic particle velocity node of an acoustic cross-mode, with acoustic pressure amplitude dependence on the cylinders' proximity to the acoustic particle velocity antinode of the excited resonance mode. Phase-locked particle image velocimetry measurements indicate that the acoustic resonance excitation synchronizes the isolated wakes of the cylinders according to their relative phase with the acoustic particle velocity at the cylinder axis plane. Notably, such effect is absent for cylinders with wakes shed at the acoustic particle velocity nodes of a resonant mode. Investigation of the phase between cylinders' wakes during resonance excitation for individual instants shows that the synchronization is not a perfect lock-in, but a statistical tendency of the wakes to shed vortices at a preferred phase, suggesting that the strong acoustic field engages in constructive or destructive interference with the shed vortices according to their phase. The results presented in this paper prove that the effectiveness of cylinder removal from certain locations in a tube bundle as a method to suppress resonance excitation may be reduced as other cylinders at large spacing may act in sync to excite acoustic cross-modes.

✉ Mahmoud Shaaban
mahmoud.shaaban@ontariotechu.net

[1] Aeroacoustics and Noise Control Laboratory, University of Ontario Institute of Technology, Oshawa, ON, Canada

Published online: 22 September 2021

Graphic abstract



List of symbols

δ	Total mode energy
ω_z	Vorticity magnitude in the x–y plane
$\overline{u'v'}_c$	Reynolds shear stress of coherent periodic structures
ϕ	Phase angle
φ	Phase difference
a	Temporal coefficient of orthogonal mode
B	Cylinder span
D	Cylinder diameter
f	Frequency
$f_{a,i}$	Frequency of the ith acoustic cross-mode
L_r	Wake closure length
M	Mach number
p_{rms}	Root-mean-square acoustic pressure
p_i	Acoustic pressure of the ith acoustic cross-mode
Re	Reynolds number
St	Strouhal number
T	Cylinder transverse spacing
U	Average flow velocity
u', v'	Streamwise and crosswise flow velocity fluctuations
u'_c	Coherent periodic velocity fluctuations
u'_r	Random velocity fluctuations
u, v	Streamwise and crosswise flow velocity
$\overline{u'v'}$	Reynolds shear stress
$\overline{u'v'}_r$	Random component of the Reynolds shear stress
U_∞	Upstream flow velocity
U_r	Reduced flow velocity
v_a	Acoustic particle velocity of the transverse mode
x, y, z	Cartesian coordinates

1 Introduction

The excitation of noise and vibration can pose hazardous operation conditions and may result in operation interruption and in some cases may escalate rapidly to a catastrophic failure (DeBoo et al. 2007; Hambric et al. 2006). Flow-induced acoustic resonance has been reported as a source of severe noise and vibration which represents a design challenge in many engineering applications such as tube bundles in heat exchangers and boilers (Blevins and Bressler 1993; Oengören and Ziada 1998; Shaaban and Mohany 2019a), turbomachines (Clark et al. 2015; Fiquet et al. 2020), air conditioning systems (Jeong 2017), cavities (Shaaban and Mohany 2015; Xu et al. 2017), combustion chambers (Rashwan et al. 2020), safety relief valves in nuclear power plants (Uchiyama and Morita

2017; Semrau et al. 2019), pipelines and side branches (Lato and Mohany 2019; Wang and Liu 2019), and several other applications (Ziada 2010). A significant generation of acoustic energy can be sustained when periodic flow instabilities couple with an acoustic mode leading to acute noise that is often associated with excessive vibrations. For tightly packed arrangements of cylinders, Ziada et al. (1989b) showed that resonance excitation is only expected if the cylinders are spaced at a transverse spacing sufficient for unstable flow patterns to form in the flow lanes. On the other hand, Arafa and Mohany (2016) observed that large transverse separation of the cylinders may lead to an enhancement of the acoustic resonance excitation, which can lead to dangerous underestimations of acoustic resonance self-excitation.

The flow–acoustic coupling mechanism that leads to resonance excitation is relatively well understood for the case of a single cylinder in cross-flow (Mohany and Ziada 2009a, b; Shaaban and Mohany 2020). Vortex shedding downstream of the cylinder acts as a source of periodic flow perturbation that occurs at a frequency corresponding approximately to a constant Strouhal number:

$$St = \frac{fD}{U_\infty}. \tag{1}$$

Periodic vortex shedding can couple with the acoustic modes that are oriented so that their acoustic particles oscillate in the same direction of flow perturbation. This is the case for the cross-modes of a rectangular duct which have particle velocity nodes on the duct walls parallel to the cylinders' axes. Due to this arrangement, the flow perturbation can provide energy to the acoustic mode leading to enhanced acoustic oscillations, which in turn enhances and organizes the vortex shedding process in a feedback cycle. The sustainable energy transfer between the acoustic field and the flow field results in a persistent resonant condition in which the two fields become coupled and locked-in to the same frequency (Mohany and Ziada 2005; Blevins 1985; Hong et al. 2020). In addition, the frequency of the cross-modes at higher oscillation amplitudes is lower than the cutoff frequency of the duct because of added mass effects of the coupled field (Shaaban and Mohany 2019b). As a result, the acoustic energy becomes trapped in the vicinity of the cylinder leading to severe acoustic amplitudes limited only by the viscous dissipation at the walls and acoustic radiation losses of the duct (Afifi and Mohany 2020). The current understanding of acoustic resonance excitation mechanism by periodic flow for compounded cylinder configurations still lacks critical information regarding the feedback effect of the acoustic field on multiple oscillating flow patterns, which is vital to understand how resonance is excited and sustained.

The flow around side-by-side cylinders has attracted considerable research interest because of its significance in many practical applications. It is well acknowledged that the periodic flow features in the wake depend primarily on the transverse spacing over a wide range of Reynolds number. For a very small spacing of $T = 1.2D$, the two cylinders behave as one structure, generating a single vortex street (Sumner et al. 1999). For $1.5D \leq T \leq 2.0D$, two different flow regimes are observed. In one regime, the wakes of the cylinder are of different width and switch in a bistable mode. In the second regime, the cylinders shed two streets of vortices that are either in phase or out of phase (Wadcock 1973). At transverse spacings $T \geq 2.0D$, two distinct vortex streets are observed (Ishigai et al. 1972). Considerable research has focused on aspects of the flow behind side-by-side cylinders at low transverse spacing. Zhou (2003) experimentally investigated the flow behind three side-by-side circular cylinders at a center-to-center spacing $T = 1.5D$. They observed that the vortical structures in the narrow wakes may be generated from the shear layer separation at the upper or the lower cylinder, while those in the wide wake may originate from the shear layer instability undergoing a transition from a jet oscillation toward the formation of vortices in individual shear layers, similar to that observed in a cavity excited by a grazing jet flow (Dequand et al. 2003).

Lee et al. (2012) investigated the wake dynamics downstream of two side-by-side cylinders of unequal diameter spaced by a gap-to-diameter ratio of 0.75. They observed that vortex shedding can lock in to the cylinder rotary excitation. At low Reynolds numbers and intermediate gap ratios, Bai et al. (2020) numerically observed asymmetric flow structures from two side-by-side cylinders. Investigations of the flow patterns downstream of side-by-side cylinders at center-to-center transverse spacing ratios of more than 3.5 diameters are scarcely reported in the literature due to a general agreement that such patterns are not correlated and can generally be assumed to follow the general behavior of single cylinders. However, the current study provides evidence that acoustic resonance excitation may change this behavior under certain conditions.

Acoustic resonance excitation has been reported for side-by-side arrangements of cylinders. Ziada et al. (1989a) showed that very tight transverse spacing does not allow the formation of the unstable periodic flow patterns responsible for resonance excitation. At moderate transverse spacing, Mohany et al. (2014) reported that acoustic resonance eliminates bistable periodic flow features in favor of a single vortex shedding frequency, indicating that the aerodynamic correlation of vortex shedding between the proximate side-by-side cylinders is enhanced by the acoustic oscillation. On the other hand, Hanson et al. (2009) reported that side-by-side cylinders at a spacing of more than 3 cylinder diameters shed vortices at a frequency similar to that of a

single cylinder at a random phase. For such isolated cases, von Kármán vortices can only be generated in synchronization using complex active control methods, such as the use of synchronized rotational motion (Rockwood and Medina 2020). Interestingly, resonance excited by aerodynamically isolated side-by-side cylinders showed unexplained features. Arafa and Mohany (2016) reported that the spacing and the location of the cylinder have a significant effect on the excitation of acoustic resonance. They reported an enhancement of the acoustic field due to the presence of more cylinders, which signals that the self-excitation of acoustic resonance may have an effect on the flow field and the phase of the shed vortices. Remedies to acoustic resonance excitation in tube bundles often employ the removal of tubes close to the acoustic velocity antinodes (Zdravkovich and Nuttall 1974). As a result, the effectiveness of this method can be diminished under certain arrangements and flow conditions. Therefore, understanding the flow characteristics that lead to this enhancement during self-excitation of acoustic resonance is important to avoid initiating or exacerbating noise problems.

This study aims to provide a clear understanding of the influence of acoustic resonance excitation on the flow field downstream of side-by-side cylinders at large transverse spacing. The aeroacoustic response, the dynamic flow characteristics, and the vortex street topology in the wake of different side-by-side cylinder configurations are experimentally investigated. Experiments are performed during the excitation of two acoustic cross-modes at different flow velocities to identify the effect of the acoustic particle velocity phase at different cylinders' locations on the acoustic–flow coupling mechanism.

2 Methodology

Figure 1 shows a simplified schematic of the test section used to carry out the experimental investigation in this work. Measurements of acoustic pressure amplitude and particle image velocimetry are carried out in an open-loop wind tunnel, where air flow is driven into a bell mouth by a centrifugal blower located at the downstream end. The test section has a rectangular cross section with a width $B = 127$ mm and a height $H = 254$ mm. Assuming a one-dimensional pressure distribution, the theoretical resonance frequency for the two modes is $f_{a,1} = 675$ Hz and $f_{a,2} = 1350$ Hz, which are in good agreement with the experimentally measured values. Air at room temperature is drawn into the wind tunnel through a bell mouth which delivers uniform air velocity profile at the test section, where configurations of side-by-side cylinders are installed.

The aeroacoustic response and the characteristics of the flow cycle during acoustic resonance are investigated

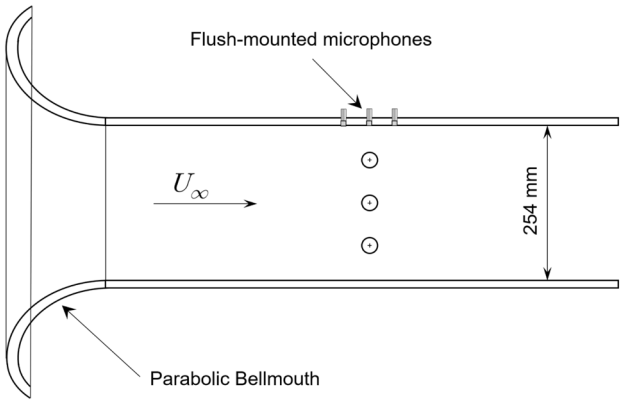


Fig. 1 A schematic drawing of the middle streamwise symmetry plane of the test section

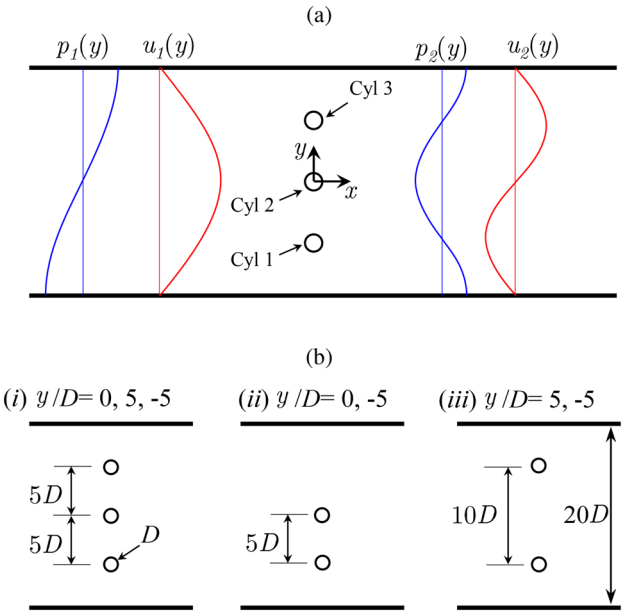


Fig. 2 **a** Distribution of the acoustic pressure and acoustic particle velocity for the first two acoustic cross-modes of the duct and **b** the investigated configurations

for configurations of two and three cylinders as shown in Fig. 2b. Cylinders of equal diameter $D = 12.7$ mm are rigidly attached side-by-side spanning the test section width $B = 127$ mm, with an aspect ratio of 10 to avoid any significant end effects. The dimensions of the cylinders are selected within the typical tube sizing used in heat exchange applications, and the test section dimensions enable the self-excitation of acoustic resonance at adequate conditions for accurate pressure and flow measurements. The transverse spacing between the cylinder axes in configurations (i) and (ii) in Fig. 2b is 63.5 mm, equivalent to $5D$, and is 127 mm for configuration (iii), equivalent to $10D$. Therefore, the

cylinders in all configuration are not in proximity and are not aerodynamically correlated. The flow perturbation due to the vortex shedding downstream of the cylinders occurs in the y direction normal to both the cylinder z axes and the flow direction x. Measurements of flow velocity profiles in the test section showed that the turbulence intensity does not exceed 1% at the maximum achievable flow velocity. Experiments were done at Mach numbers up to 0.35 to avoid transonic flow in the vicinity of the cylinder (Shapiro 1953).

The profiles of acoustic pressure $p(y)$ and acoustic particle velocity $u_a(y)$ are shown schematically in Fig. 2a. The fundamental acoustic cross-mode has two pressure antinodes on the walls parallel to the cylinders' axes and one acoustic particle velocity antinode at the mid-height. The second acoustic cross-mode has three pressure antinodes and two acoustic velocity antinodes. Acoustic pressure measurements are carried out using 1/4-inch pressure microphones (PCB model 377A12), flush mounted at the top wall of the test section. The microphones are attached to an antinode of the acoustic pressure corresponding to the excited acoustic cross-modes. The signal is recorded at a sampling rate of 20 kHz for 60 s. To obtain the spectral characteristics of the signal, a fourth-order bandpass filter is applied over a band of 20 Hz around the dominant tonal peak to identify the root-mean-square acoustic pressure excited by vortex shedding. Welch's overlapped segment averaging estimator is then blocked into samples of 1 s, and the ensemble average is calculated with a Hanning window at 50% overlap (Stoica and Moses 2005). The uncertainty in the acoustic pressure measurements is estimated assuming a Gaussian distribution of real error to be less than 1%. The resulting spectra have a resolution of 1 Hz, and the frequency at the peak acoustic pressure is manually identified with an uncertainty of 0.5 Hz.

A schematic of the setup used to carry out particle image velocimetry (PIV) is shown in Fig. 3. Both random and phase-locked PIV measurements are carried out at the streamwise x–y plane to measure the flow velocity vectors during excitation of the acoustic cross-modes. A pulsed Nd:Yag laser with a wavelength of 532 nm is used to illuminate the flow field. A CCD camera is used to capture images with a resolution of 2752 pixel × 2200 pixel. The air flow is seeded with di-ethyl-hexyl-sebacate (DEHS)) particles of a mean diameter of 1 µm. The PIV measurements are carried out at flow velocities that induce peak resonance excitation for the first and the second acoustic cross-modes and at a flow velocity of 20 m/s with no acoustic resonance excitation. The time between pulses is adjusted to capture the maximum particle displacement within one-quarter of the final interrogation window used for vectors calculation, which is performed using a multipass cross-correlation algorithm with one pass at initial window size 64×64 pixels^2 with 50% overlap and four final passes at interrogation window size 32×32 pixels^2 with 50% overlap. The vorticity in the x–y plane is measured from vectors of velocity using a second-order least-squares differential scheme. The final vector field is obtained with a resolution of $0.1D \times 0.1D$. The uncertainty in the flow quantities is evaluated using the correlation statistics method (Sciacchitano and Wieneke 2016). The maximum uncertainty in the velocity and vorticity measurements is estimated to be 2.3% and 7%, respectively.

During phase-locked measurements, the signal from the flush-mounted microphone at the acoustic pressure antinode of the test section is used to trigger the laser pulse and take a

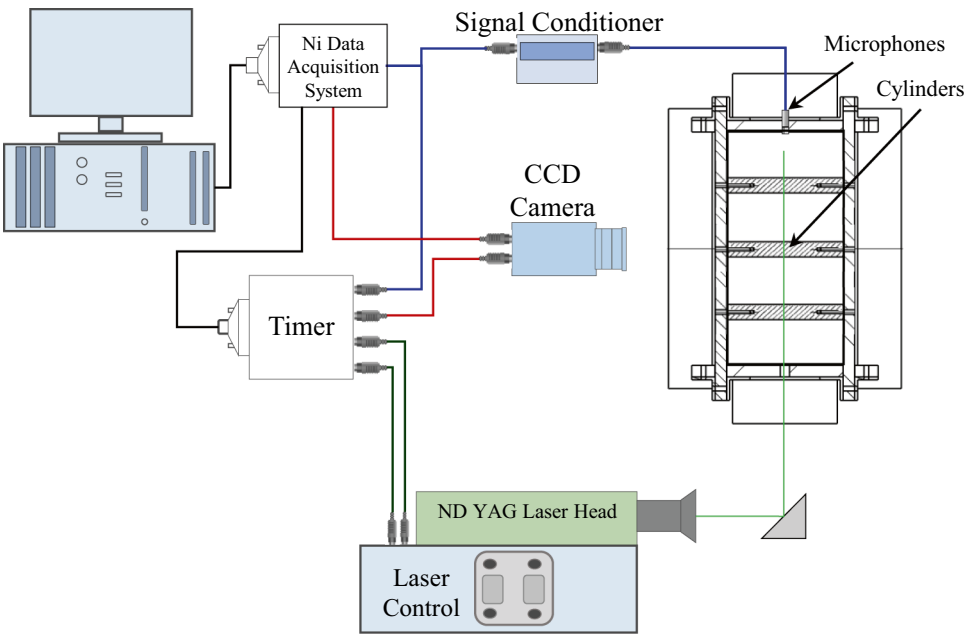


Fig. 3 A schematic of the particle image velocimetry setup

number of images at the same phase of the acoustic pressure cycle. Eight sets of measurements are taken at eight uniformly spaced phases of the acoustic pressure cycle. At the same phase angle, 250 instantaneous images are acquired. Velocity vectors are averaged for the 250 instants at the same phase for each configuration, discarding any point where less than 200 vectors are validated.

3 The effect of the cylinder location on aeroacoustic resonance excitation

The configuration of side-by-side cylinders in cross-flow resulted in a distinctive aeroacoustic response to the flow velocity and the cylinders' configuration. The effect of the flow velocity on the spectral characteristics of the acoustic pressure is shown in Fig. 4 for the three configurations illustrated in Fig. 2, in addition to the cases of a single cylinder in mid-height at $y = 0$ and a single cylinder at $y = 5D$ as a basis for comparison. For all configurations, the increase in flow velocity was accompanied by a respective increase in the frequency of an acoustic pressure peak corresponding to the vortex shedding frequency. The Strouhal number pertaining to this peak is St = 0.20, in agreement with the value of vortex shedding from a single cylinder at $\mathrm{Re} = 2 \times 10^4$ to 12×10^4. In Fig. 4, the frequencies of the acoustic cross-modes are visible as nearly vertical lines at frequencies of 675 Hz and 1250 Hz.

The excitation of acoustic resonance is visible in Fig. 4 in the form of localized episodes of significantly higher acoustic sound pressure level, observed at the coincidence of the vortex shedding frequency with one or more acoustic mode frequencies. For a single cylinder installed at $y = 0$, the flow velocity perturbation induced by vortex shedding is able to couple with the acoustic field to excite the first cross-mode at a reduced flow velocity $U_r = 5.2$, at a lock-in frequency $f_{a,1} = 675$ Hz. The second acoustic cross-mode is not excited because the cylinder is located at the acoustic particle velocity node of that cross-mode. When the cylinder is located at $y = -5D$, a significant sound pressure level is observed over $U_r = 9$–11.5, due to the excitation of the second acoustic cross-mode with $f_a = 1310$ Hz. As more cylinders are added, the acoustic response exhibits features related to the position of the cylinders and their interaction with the acoustic cross-modes. The configuration of three side-by-side cylinders in Fig. 4e induces the highest acoustic pressure amplitudes for the first and the second acoustic cross-modes. The acoustic mode frequency at resonance is slightly different for each configuration. The deviation from the theoretical value calculated for the duct with no cylinders and no-flow is affected by two major factors. First, the presence of

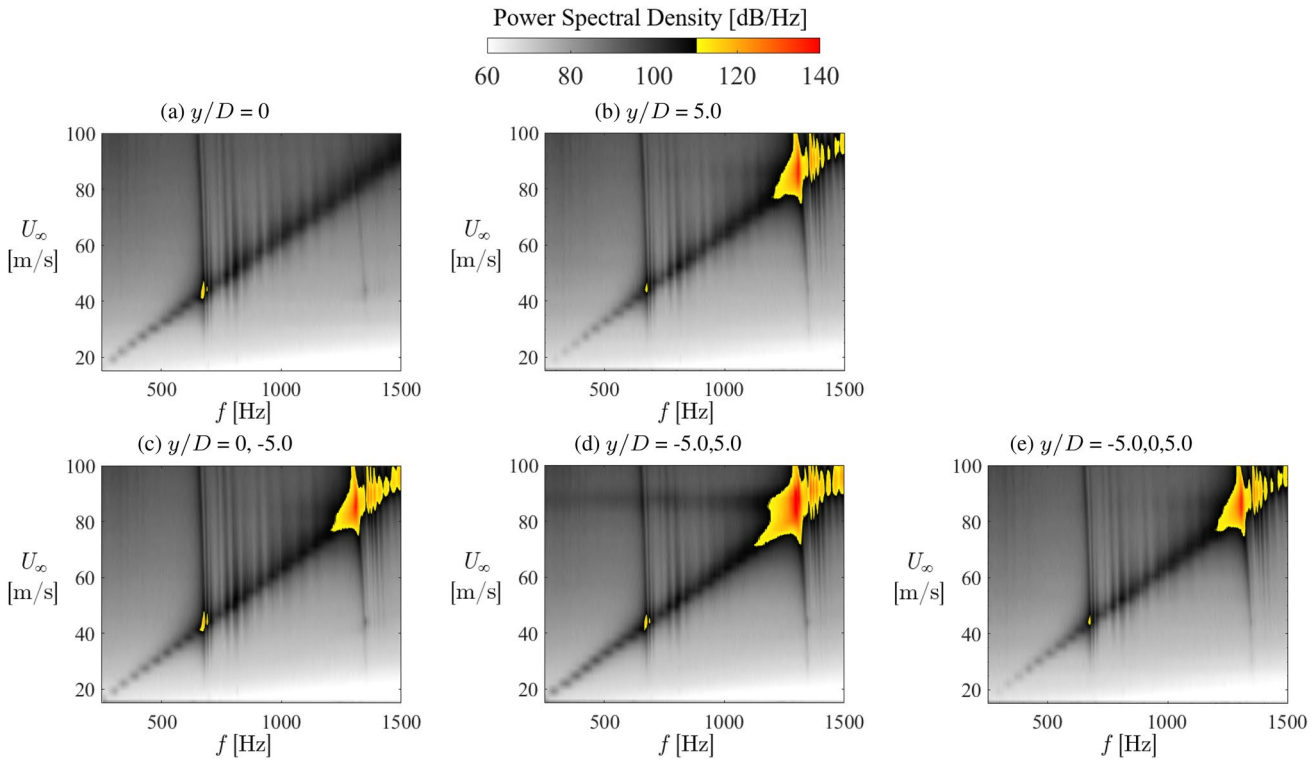


Fig. 4 Spectral characteristics of the acoustic pressure signal at different flow velocities for different configurations of side-by-side cylinders with $D = 12.7$ mm

cylinders in the duct restricts the path of acoustic particles between the boundaries of the duct so that the acoustic particle velocity is increased in the vicinity of the cylinders causing an added mass effect that decreases the acoustic mode frequency. Moreover, the flow velocity results in a convective effect that results in a longer apparent path of the acoustic particles, causing a further decrease in the acoustic mode frequency (Shaaban and Mohany 2019b). For the case of two cylinders, the amplitude of resonance for the first acoustic mode increases if a cylinder is at mid-height, while the second acoustic mode amplitude is enhanced if the cylinders are located at $5D$ from the two walls, i.e., at the two acoustic particle velocity antinodes of the second cross-mode. This is quite interesting since the acoustic particle velocity at these locations is 180° out of phase for the second acoustic cross-mode. Excitation of acoustic resonance requires a strong organized flow field with correlated oscillations. As vortex shedding from aerodynamically isolated cylinders is generally not correlated, one would expect that the randomly aligned vortices would result in acoustic sources that statistically weaken resonance excitation. The observation from Fig. 4d shows that this is clearly not the case and suggests a constructive interference between the vortex shedding downstream of the cylinders and the acoustic cross-mode to produce stronger sound sources.

The acoustic pressure p_{rms} is plotted against the reduced flow velocity U_{r} in Fig. 5 for the case of three side-by-side cylinders.

$$U_{\mathrm{r}} = \frac{U_{\infty}}{f_{\mathrm{a,1}} D} \tag{2}$$

The reduced velocity uses the first acoustic cross-mode frequency $f_{\mathrm{a,1}}$ for normalization, so that the coincidence between the first acoustic cross-mode and the vortex shedding mode occurs at $\mathrm{St} \times U_{\mathrm{r}} = 1$. Each point in Fig. 5 represents the amplitude and the frequency of the vortex shedding component taken from the pressure spectrum.

At two ranges of reduced velocities around $U_{\mathrm{r}} = 5$ and $U_{\mathrm{r}} = 10$, a substantial increase in the acoustic pressure is observed. At $U_{\mathrm{r}} = 5.0$, the acoustic pressure increases to $p_{\mathrm{rms}} = 0.16$ kPa for the first acoustic cross-mode, compared with $p_{\mathrm{rms}} = 1.4$ kPa at $U_{\mathrm{r}} = 10$ for the second acoustic cross-mode. This substantial increase is mainly attributed to the availability of a higher flow kinetic energy. The ratio of the peak frequency to the first acoustic mode frequency is plotted in Fig. 5. A linear increase in a single peak follows the behavior of a single cylinder at a Strouhal number of $\mathrm{St} = 0.20$, deviating only to keep a constant frequency over a range of reduced velocities during the lock-on condition. The observation of only a single vortex shedding peak indicates that the three cylinders shed

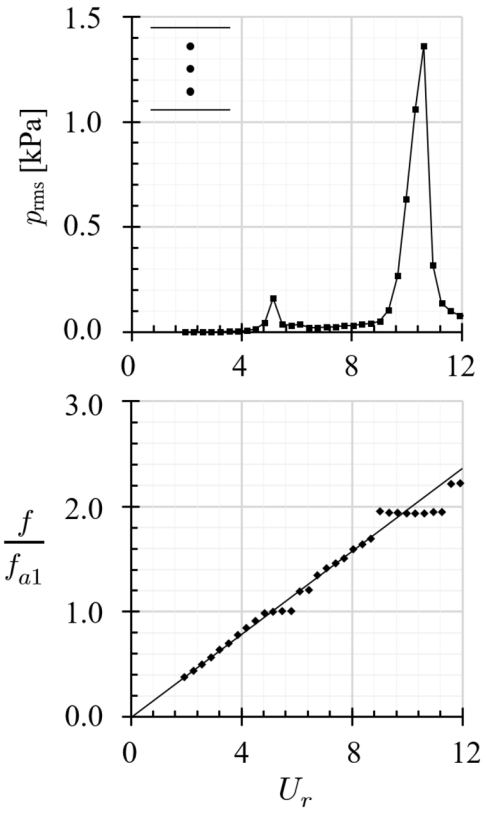


Fig. 5 The aeroacoustic response of three aerodynamically isolated side-by-side cylinders in cross-flow

vortices at the same frequency. The presence of more side-by-side cylinders in the configurations may excite additional acoustic resonance regions, but it does not impact the lock-in ranges.

The effect of the cylinders' configuration on the pressure amplitude is evident in Fig. 6. In the four configurations shown in Fig. 6, the first acoustic cross-mode is excited at $U_{\mathrm{r}} = 5.0$, reaching an acoustic pressure $P_{\mathrm{rms}} = 0.1$ kPa. On the other hand, the excitation of the second acoustic cross-mode at $U_{\mathrm{r}} = 10$ is dependent on the cylinder configuration. Particularly, the presence of a cylinder at mid-height does not contribute to the excitation of the second mode. For instance, the acoustic pressure at the peak of the second cross-mode is approximately at the same level of $p_{\mathrm{rms}} = 0.5$ kPa for the case $y = -5D$ and the case $y = 0$ and $-5D$. At the mid-height of the test section, the vortex shedding coincides with an acoustic particle velocity node of the second acoustic cross-mode, as shown in Fig. 2a. Therefore, it is not possible to provide the excitation of acoustic velocity at this location in the absence of an acoustic field component. On the other hand, the second mode can be enhanced by the presence of additional cylinders away from the mid-height, as in cases $y = -5D$ and $5D$ in Fig. 6, and for $y = -5D$, 0, and $5D$ in Fig. 5. For these cases, the

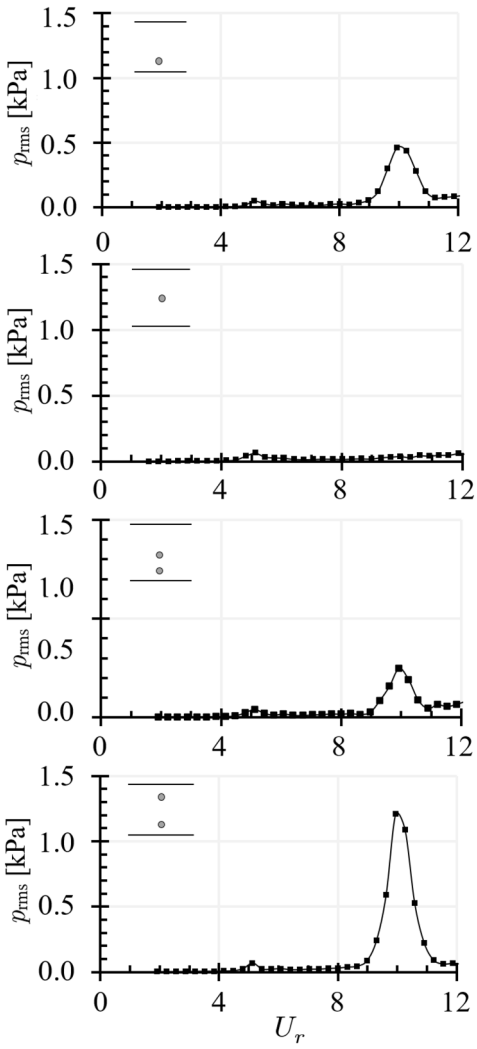


Fig. 6 The acoustic pressure at different reduced flow velocities for different configurations

acoustic pressure increases to $p = 1.2$ kPa, slightly more than double its value for only one cylinder. This increase can be attributed to the quadratic increase in the visco-thermal losses, compared with a third-order increase in the sound source power at the higher flow velocity. The configuration of the cylinders had no effect on the reduced velocity at resonance excitation, nor on the lock-in region, suggesting that the wakes do not interact in any way that changes the vortex shedding frequency.

4 Vortex dynamics in the wake during acoustic resonance

As evident from the previous discussion, the aeroacoustic response of different side-by-side cylinders' configurations in cross-flow indicates a phase correlation between aerodynamically isolated cylinders driven by acoustic resonance excitation. Such correlation is vital to the acoustic resonance excitation mechanism, as a favorable phasing between vortex shedding would ensure that sound sources that sustain acoustic resonance are aligned to be most effective. This discussion provides clear indication of this correlation and demonstrates its dominant features by identification of the flow field characteristics with and without the self-excitation of acoustic resonance. For an unsteady flow, the mean flow is an artificial construct, but it remains useful as an analytical tool representing a base flow over which the motion of vortex structures is superimposed. The normalized streamwise velocity contours are presented in Fig. 7 for three side-by-side cylinders at three different flow velocity conditions. At $U_\infty = 20$ m/s, acoustic resonance was not present due to the absence of the coincidence condition. The peaks of the first and the second acoustic cross-modes were observed at flow velocities of $U_\infty = 44$ m/s and 85 m/s, respectively. The configuration of cylinders had no substantial effect on the average features of the flow field. Results shown in Fig. 7 indicate that the increase in the flow velocity as well as the acoustic pressure amplitude did not change the width of the wakes downstream of the cylinders and did not induce any aerodynamic interaction between the cylinders that is not present in the case of no acoustic resonance. Although the presence of the cylinders results in the entrapment of the flow and an increase in the streamwise flow velocity in their proximity region, the wakes of the cylinders do not interact downstream of the cylinders. Consequently, the increase in the acoustic pressure is expected to be driven purely by the phasing relationship with the acoustic field that would not be visible in averaged data.

The increase in the flow velocity has an important effect on reducing the closure length of the recirculation zone downstream of the cylinders. The effect of Reynolds number on the closure length L_r is shown in Fig. 8. The closure length is defined as the length between the center of the cylinder and the location where the average streamwise velocity $u_x = 0$ directly downstream of the cylinder axis (Norberg 1998). Results show a good agreement with the results of infinite cylinders in cross-flow in the absence of any acoustic excitation. The increase in Reynolds number resulted in a decrease in the closure length. The closure length dropped from around $L_r = 2D$ at $\mathrm{Re} = 1.5 \times 10^4$ to $L_r = D$ at $\mathrm{Re} = 10^5$, which indicates that the wakes of the cylinders on average behave as aerodynamically isolated, with minimal effect of the acoustic resonance excitation on the average flow field. The formation of vortices closer to the cylinder wall is consistent with the increase in acoustic pressure for the second acoustic cross-mode, as the interaction of the higher vorticity field with the cylinder wall would result in higher production of acoustic power (Alziadeh and Mohany 2018).

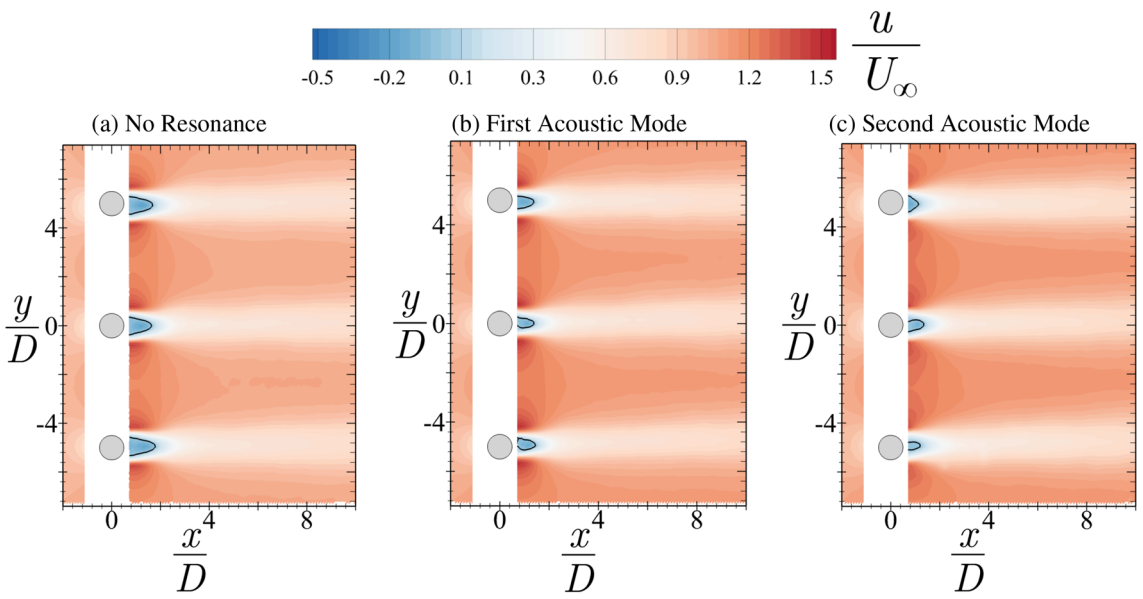


Fig. 7 Average normalized streamwise flow velocity contours for three side-by-side cylinders at **a** no acoustic resonance, $U_\infty = 20$ m/s, **b** the peak of the first acoustic cross-mode resonance, and **c** the peak of the second acoustic cross-mode resonance. The solid black line is plotted at $u_x = 0$ to indicate the recirculation zone

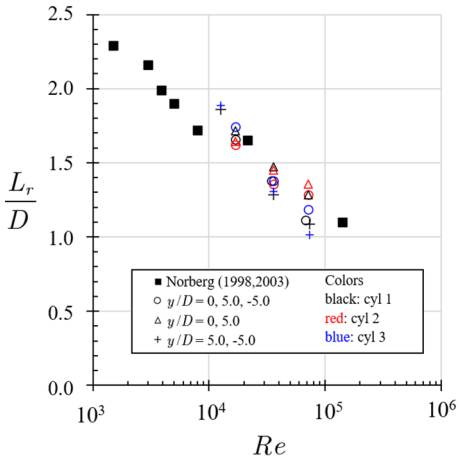


Fig. 8 Length of recirculation zone closure L_r compared with the data of Norberg (1998), Norberg (2003)

While the average flow field is not affected by the acoustic resonance, the dynamic features of the vortex shedding cycle clearly elucidate the effects of resonance excitation on the flow field. In Figs. 9 and 10, the normalized vorticity field ω_z in the x–y plane is shown at four equally spaced instants over the locked-in flow–acoustic cycle at the peak resonance excitation of two different acoustic cross-modes. The phase angle $\phi = 0$ corresponds to the instant at which the acoustic pressure on the upper test section wall crosses zero and increases. On the left side of each flow field in Figs. 9 and 10, vectors of acoustic particle velocity v_a show the instantaneous direction and relative amplitude at three chosen planes at $y/D = -5.0$, 0, and 5.0. The behavior of the v_a vectors complements the distribution shown earlier in Fig. 2a. Over the cycle, the v_a vectors reach their maximum amplitude at $\phi = 0°$ and 180° and become zero at $\phi = 90°$ and 270°. For the first acoustic cross-modes, vectors at the three planes are all in phase. For the second acoustic cross-mode, the v_a vectors are out of phase at $y/D = -5.0$ and 5.0, while the acoustic particle velocity at the nodal plane $y/D = 0$ is zero at all phases.

Figure 9 clearly demonstrates that the phase-locked vortex shedding cycle is influenced by the self-excitation of acoustic resonance. Not only is the shedding synchronized to the same exact frequency, but it is also at the same phase. During the excitation of the first acoustic cross-mode, the three cylinders shed vortices that are in phase with each other. The vortices are separated at the same instant and are conveyed in parallel synchronized paths downstream. The vortices in each wake do not interact with the vortices of other wakes, suggesting that the synchronization is not imposed by any aerodynamic interaction.

The cycle of vorticity during the second acoustic cross-mode excitation is shown in Fig. 10. At each phase, vortices shed in the wakes of the cylinders at $y/D = -5.0$ and 5.0 and are antisymmetric. Notably, that is also the case for the acoustic particle velocity vectors v_a at the two planes. The third cylinder at $y = 0$ shows no distinctive pattern of vortex shedding, indicating that vortices are not shed with a constant phase with respect to the acoustic pressure. Therefore, the phase of vortex shedding downstream of the cylinder at mid-height is not correlated with the phase of the acoustic

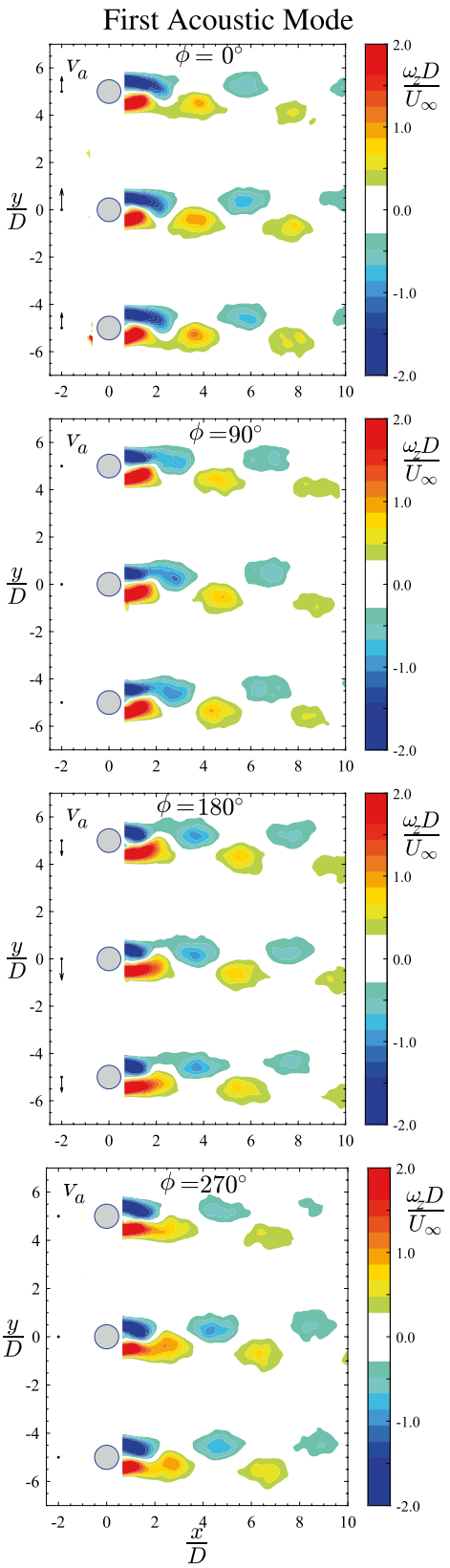


Fig. 9 Normalized phase-locked vorticity contours for the case of three cylinders at four equally spaced instants during the resonant cycle of the first acoustic cross-modes

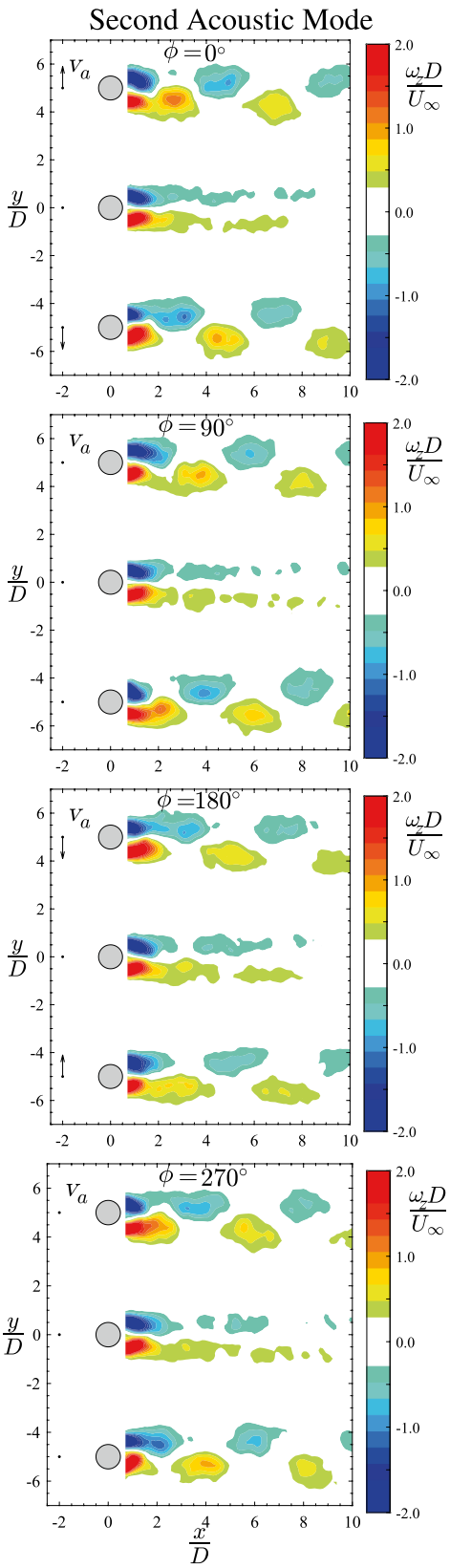


Fig. 10 Normalized phase-locked vorticity contours for the case of three cylinders at four equally spaced instants during the resonant cycle of the second acoustic cross-modes

cycle. The cylinder at $y/D = 0$ acts as an aerodynamically isolated cylinder in a similar behavior expected for the case with no flow–acoustic coupling.

In Fig. 11, the phase-locked vorticity field downstream of the investigated arrangements of side-by-side cylinders is compared at the point of maximum acoustic particle velocity amplitude in the direction of the upper wall. In affirmation of the mechanism characteristics discussed above, the first acoustic cross-mode results in synchronized vorticity shedding for the cylinders even though the wakes are not in aerodynamic proximity of each other. The consistent phase in the three cases is a clear indication that all three cylinders act as sound sources to sustain the strong acoustic field, explaining the incremental nature of the acoustic pressure p_{rms} as additional cylinders are added.

The temporal development of turbulent flow fields can be decomposed into mean and fluctuating components using Reynolds decomposition (Trip and Fransson 2017). In the context of conventional turbulence modeling, the fluctuation away from a global mean includes a contribution from the periodic large-scale motion and a contribution from local turbulence. Consider a sample population of velocity fields measured at fixed position and phase-locked to a certain instants in the cycle. The mean of all instants shows the mean velocity over which vortices are imposed. For a certain phase, the field is the periodic motion, with the vortices observed at their average position. Deviation from the ensemble average comes from two sources. First, fluctuations due to small-scale random turbulence are superimposed on the large-scale vortices. Second, there are fluctuations due to the fact that the large-scale motion itself is not the same for every vortex due to turbulent dispersion (Cantwell and Coles 1983). For the most part, the subsequent discussion will make no distinction, referring to all fluctuations away from the ensemble average at constant phase as being due to random turbulence. Because the flow is periodic in time, the flow velocity u is a contribution of three components, so that $u = U + u'_{\mathrm{c}} + u'_{\mathrm{r}}$, where U is the average velocity, u'_{c} is the periodic velocity fluctuation due to the coherent structure of vortex shedding, and u'_{r} is the random velocity fluctuation induced mainly by turbulence. As a result, the Reynolds stress is a contribution of two components: coherent and random, so that

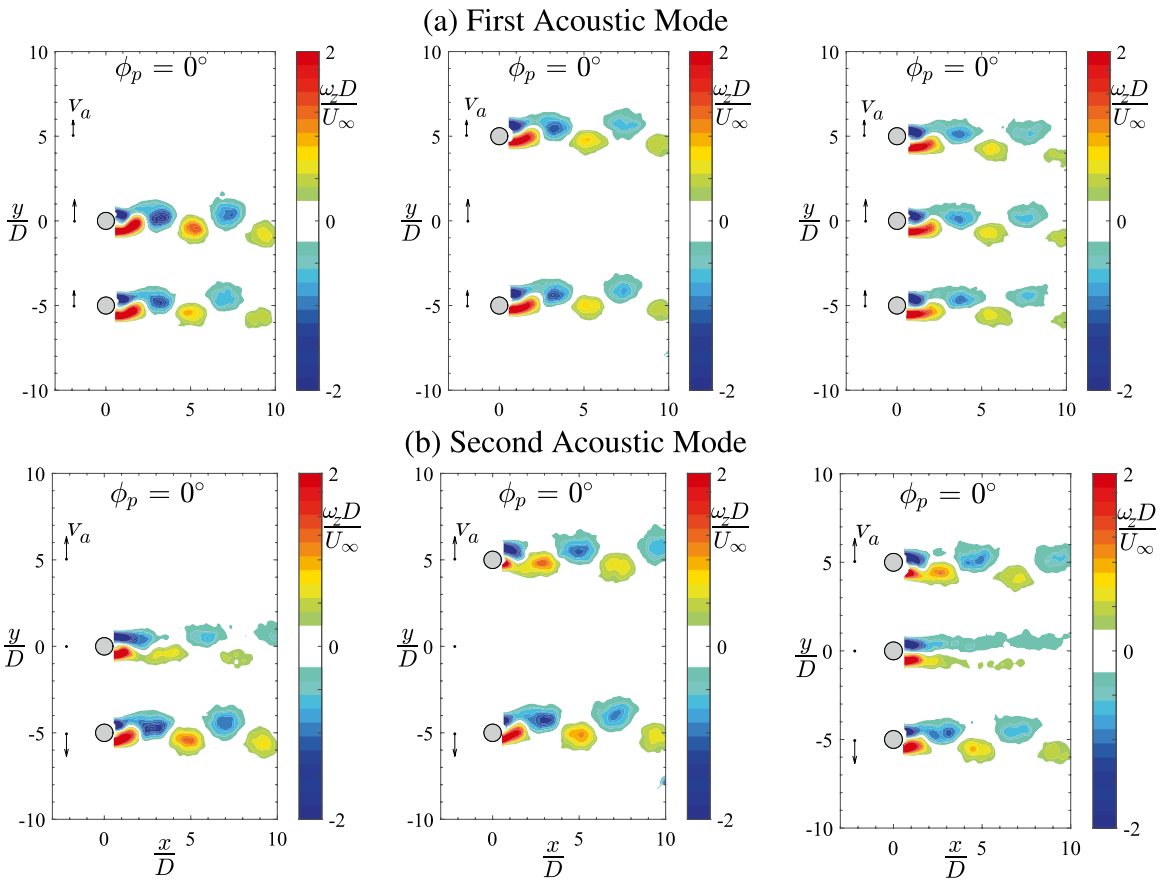


Fig. 11 Normalized phase-locked vorticity fields downstream of different side-by-side cylinders' configurations at the same phase instant of the acoustic cycle during **a** the first acoustic cross-mode resonance excitation, and **b** the second acoustic cross-mode resonance excitation

$$\overline{u'v'} = \overline{u'v'}_c + \overline{u'v'}_r \quad (3)$$

where c and r refer to coherent and random components, respectively. The coherent Reynolds stress component represents the periodic fluctuations of the periodic flow structures which are phase-locked with the acoustic cycle. In the following discussion, the coherent fluctuating components are discussed to investigate the effect of acoustic resonance excitation on the overall wake topology.

Figure 12 shows the Reynolds shear component of the coherent structures $\overline{u'v'}_c$ during the excitation of the first and second acoustic cross-modes. For the first acoustic mode, a region of significant coherent Reynolds stress is located downstream of all cylinders in the three cases, suggesting that vortex shedding in all wakes engages with the acoustic field to sustain the acoustic resonance. At higher flow velocity necessary to excite resonance of the second mode, Fig. 12b shows a distinctive absence of the coherent Reynolds shear stress $\overline{u'v'}_{,c}$ downstream of the cylinders at mid-height. Vortex shedding downstream of this cylinder still results in periodic structures as evident from the proper orthogonal decomposition results discussed next, but the periodic behavior does not persistently happen at a particular phase with the acoustic pressure cycle. Consequently, no contribution from the vortex shedding of the cylinder at mid-span to the excitation of the second acoustic cross-mode can occur.

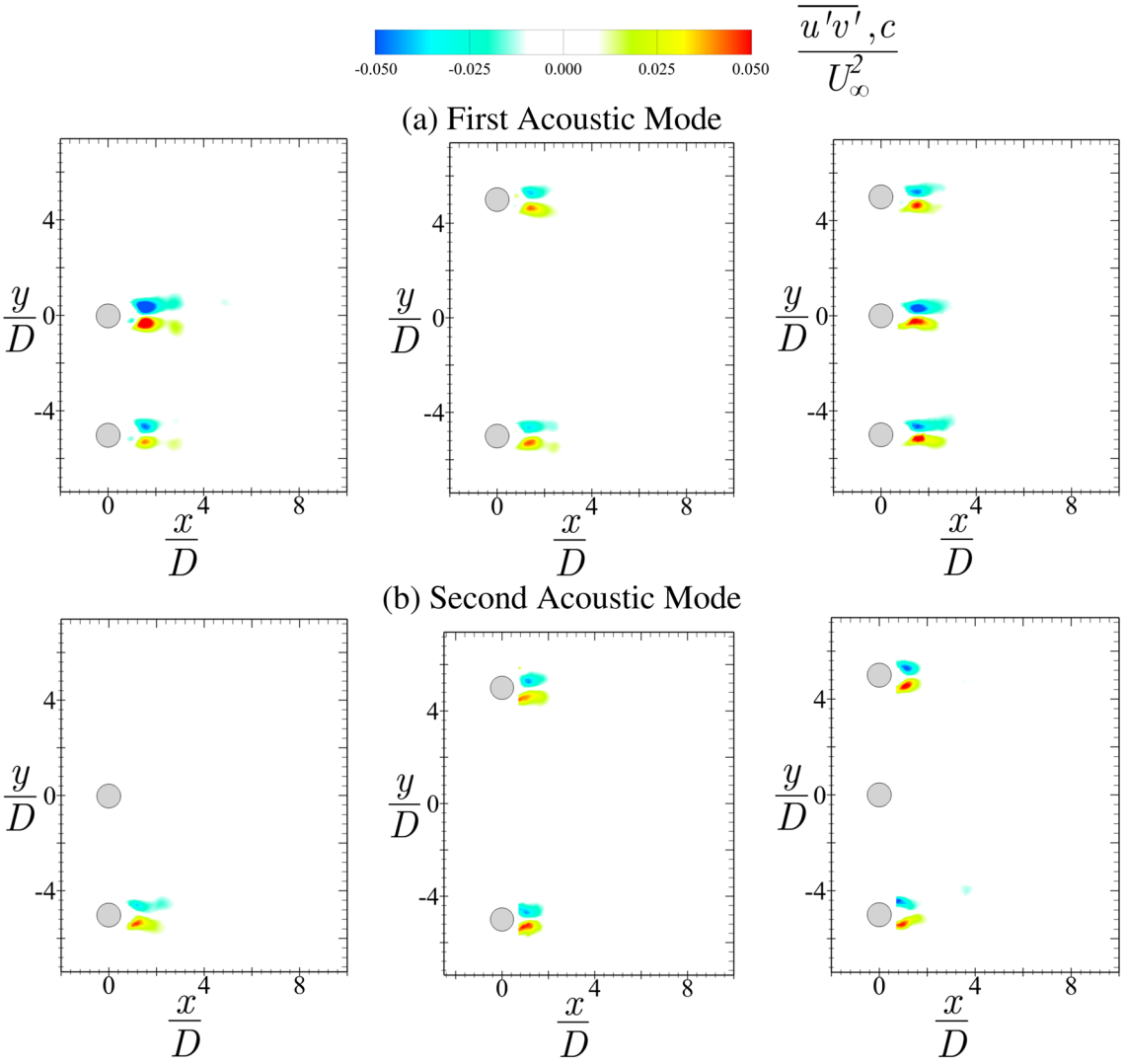


Fig. 12 Contours of periodic Reynolds shear stress $\overline{u'v'}_c$ at **a** the peak of first acoustic cross-mode resonance, and **b** the peak of second acoustic cross-mode resonance

5 Acoustic resonance effect on the temporal correlation of vortex shedding

Figure 13 shows the samples of the instantaneous patterns of vorticity for three side-by-side cylinders at the peak of the second acoustic mode excitation. Two samples are shown to illustrate the variance in the wake of this particular cylinder. Cylinders at $y/D = -5.0$ and 5.0 have an antisymmetric pattern of vorticity consisting of observations reported earlier. The cylinder located at the acoustic particle velocity node of the second acoustic cross-mode shows an inconsistent shedding phase. The cores of the vortices are at different locations with respect to the other wakes in each of the samples shown despite the constant acoustic pressure phase.

To investigate the nature of the synchronization imposed by the resonant acoustic field on vortex shedding, the temporal characteristics of the flow cycle were investigated by means of proper orthogonal decomposition (POD) for the case of three side-by-side cylinders using the method

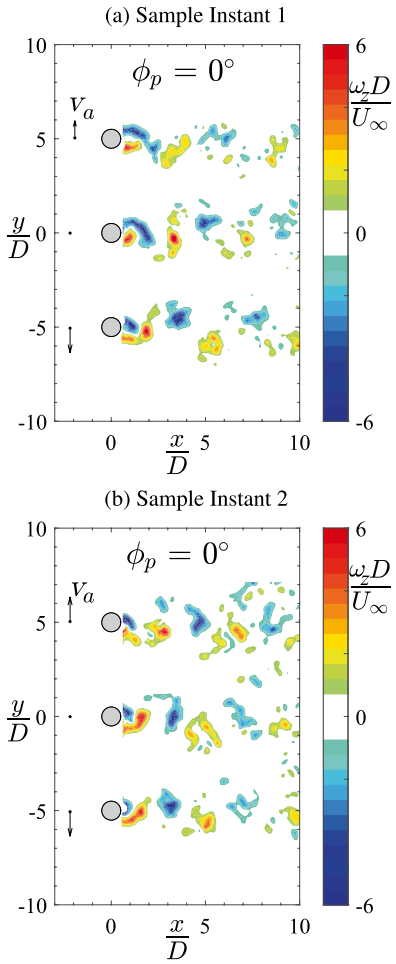


Fig. 13 Sample instantaneous patterns of vorticity for three side-by-side cylinders at the peak of the second acoustic mode excitation

illustrated in Fig. 14. Each frame was separated into three adjacent frames to calculate the temporal POD coefficients of vortex shedding for each cylinder separately. POD was applied to three groups of 1250 instantaneous velocity vector instants to represent the velocity fluctuating component in terms of orthogonal spatial modes $\mathbf{\Phi_i}(x, y)$ and their corresponding modal temporal coefficients $a_{n,k}(t)$ for each instant n, where k denotes the descending order of the mode according to its energy (Vitkovicova et al. 2020). The shedding phase angle $\phi_{\mathrm{cyl}_{m,n}}$ for cylinder m at an instant n was calculated from the temporal coefficients of the pair of orthogonal modes with the highest energy $a_{n,1}$ and $a_{n,2}$, normalized by the total energy δ as proposed by Van Oudheusden et al. (2005).

$$\tan \phi_n = \frac{a_{n,2}}{\sqrt{\delta_{n,2}}} \times \frac{\sqrt{\delta_{n,1}}}{a_{n,1}} \tag{4}$$

Figure 15 shows the phase portraits for the flow around three side-by-side cylinders before resonance excitation and during the excitation of the first and the second acoustic modes. The alternating pattern of vortex shedding results in an alternating exchange of energy between the first two POD modes, as typical for wakes of bluff bodies (Islam and Mohany 2020). As a result, the time coefficients of the two POD modes are arranged in a circular pattern. For all cases, excitation of acoustic resonance does not seem to have a significant effect on this behavior, indicating that the alternating topology of vortex shedding remains unchanged while its phase is influenced by the strong acoustic field. The phase portrait for cylinder 2 at $y = 0$ clearly indicates regular vortex shedding of typical characteristics. This is consistent with the observations at distinctive instants in Fig. 13. Therefore, there is a need to investigate the statistical characteristics of the phase difference between vortex shedding from the different cylinders.

To identify patterns in the phase of shedding between the different cylinders, Fig. 16 shows a scatter plot of the difference in vortex shedding phase between each pair of cylinders. The phase of vortex shedding downstream of cylinder 1, located at $y/D = -5.0$, is plotted on the horizontal axis, and the phase of the other two cylinders is shown on the vertical axis. Each frame appears as a single point. In a complete synchronization, all points shall fall on a single line. The prevalence of different phase difference is plotted in histograms for bands of 40° to identify any statistical tendency toward a certain value. Phase differences are scattered indicating no perfect synchronization of vortex shedding. This is expected for the case of no resonance, as shown in Fig. 16a. The histograms in this figure show no particular tendency toward any certain phase difference. However, during acoustic resonance, Fig. 16b shows two different behaviors. The

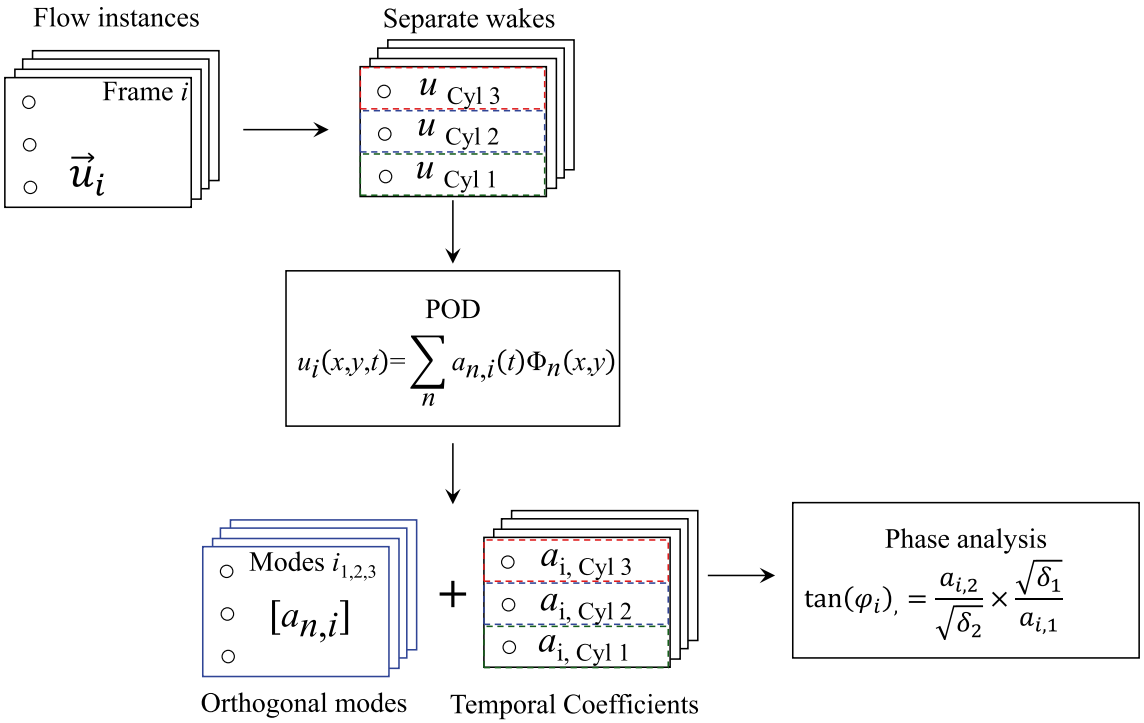


Fig. 14 Method applied to flow instances to obtain the instant vortex shedding phase in the wake of three cylinders

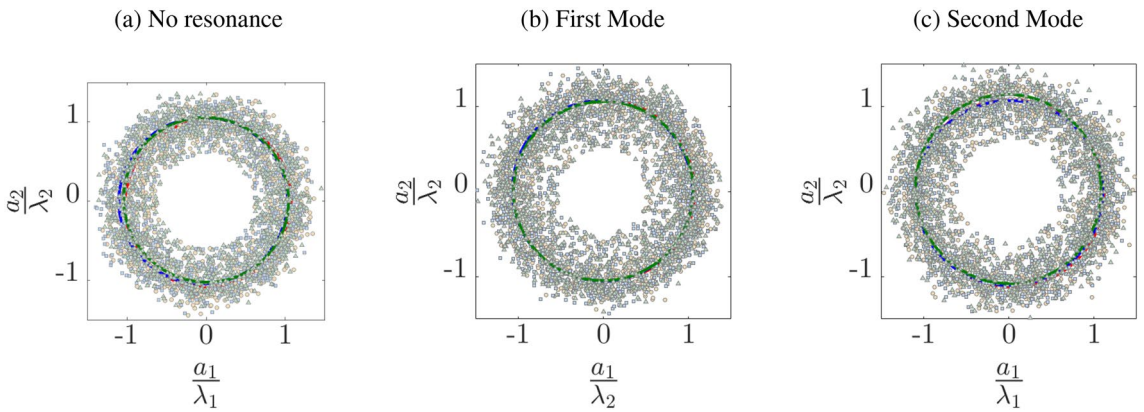


Fig. 15 Phase portrait of the first pair of POD modes temporal coefficient for the vortex shedding downstream of three side-by-side cylinders at **a** no resonance, **b** first acoustic cross-mode, and **c** second acoustic cross-mode

phase $\phi_{\text{cyl 2}}$ of the cylinder at mid-height $y/D = 0$ does not show any tendency toward any particular phase difference with the phase $\phi_{\text{cyl 1}}$ of the cylinder at $y/D = -5.0$. On the other hand, the excitation of strong resonant second acoustic mode has a distinguished effect on the phase of vortex shedding phase difference $\varphi_{13} = \phi_{\text{cyl 1}} - \phi_{\text{cyl 3}}$. Vortex shedding downstream of these two cylinders has a clear tendency toward a phase difference of 180°, consistent with the phase difference of the acoustic particle velocity. Although this tendency does not result in perfect synchronization of the vortex shedding phase at all frames, the histogram for this case shows that the effect is significant, with phase difference within 45° for 23% of the frames and 90° for 45% of the frames. The imperfect synchronization of vortex shedding suggests that the acoustic resonance does not unify the vortex shedding phase of the three cylinders, but rather interacts constructively with favorable phases and destructively with unfavorable phases. This constitutes a vital process for the feedback mechanism to influence the flow field to act in alignment with the acoustic field and sustain the energy transfer from the flow to the acoustic field.

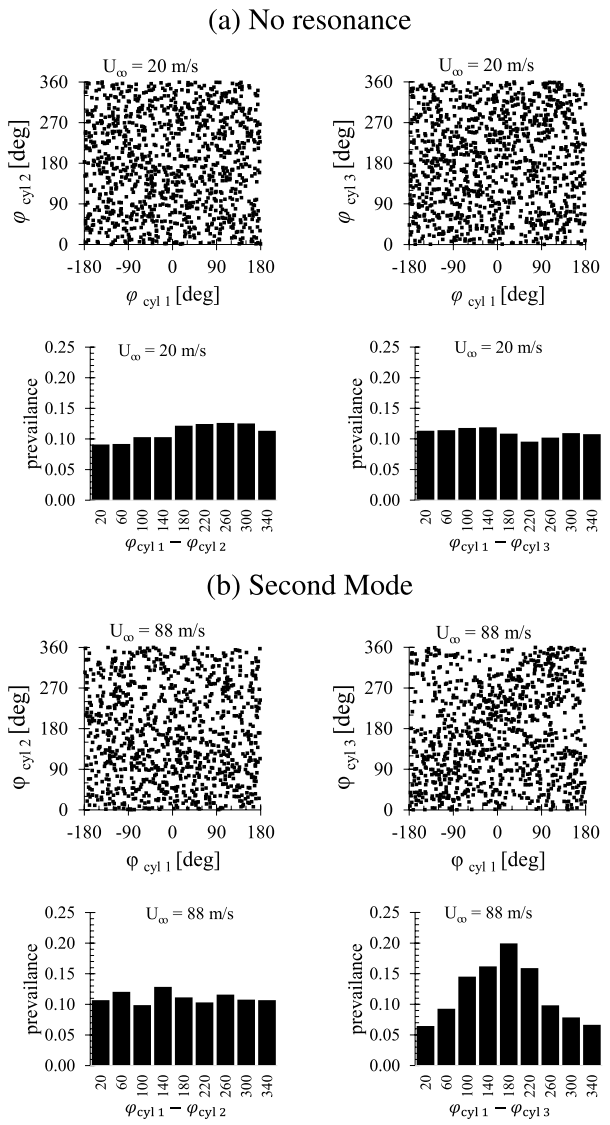


Fig. 16 Effect of the second mode resonance excitation on patterns of vortex shedding phase difference between three aerodynamically isolated side-by-side cylinders

As indicated in the foregoing discussion, a plausible explanation of the observed synchronization can be attributed to the net interaction between the strong acoustic oscillations and the vorticity field. These oscillations act against the flow velocity fluctuation if their phasing is not favorable to produce power. As a result, such instances are suppressed compared to other instants of vortex shedding with favorable phasing. As the temporal coefficients indicated, this process does not lead to a perfect alignment of all vortex shedding cycle, but rather results in a statistical preference to synchronized vortex shedding that enhances the acoustic field. Overall, this statistical tendency of the vortices toward a certain phase leads to a phasing that is consistent with the acoustic mode phase pattern on average. The presence of the acoustic field actively, but partially, suppresses shedding patterns that result in unfavorable phasing to the acoustic power generation, dictating a shedding pattern that is synchronized on average. In the case that a cylinder cannot engage in acoustic resonance excitation due to the absence of acoustic particle velocity, the shedding downstream of the cylinder would not be influenced in a similar manner. Such effects need to be taken into consideration when designing methods to control the excitation of acoustic resonance. Methods that rely on removal of certain vortex shedding sources should not assume that the other sources would be isolated because of their detachment, which may act in sync in spite of large spacing. An effective method to control acoustic resonance excited by multiple sources needs to disrupt the phasing between these sources.

6 Conclusion

In this work, the synchronization of the vortex shedding downstream of aerodynamically isolated side-by-side cylinders is experimentally investigated. Cylinders of the same diameter were subjected to cross flow at conditions that give rise to acoustic resonance excitation for the first and the second acoustic cross-modes. Acoustic pressure measurements and phase-locked particle image velocimetry were used to characterize the influence of the cylinder configuration on the excitation of acoustic resonance and the phase of the vortex shedding cycle downstream of the cylinders. The excitation of acoustic resonance had no significant effect on the topology and symmetry of individual cylinders' wakes but had a profound effect on the phase of vortex shedding. During the peak excitation of the first acoustic cross-mode, ensemble averaging of vortex shedding at the same phase showed that all cylinders shed vortices in a synchronized pattern with vortices separating in-phase downstream. On the other hand, the antisymmetric acoustic particle velocity pattern of the second mode resulted in a shedding phase difference that depends on the relative phase of the acoustic particle velocity. Cylinders with wakes aligned with the node of acoustic particle velocity did not participate in the synchronized shedding. Vortex shedding phase analysis using proper orthogonal decomposition showed that the synchronization effect is of a statistical nature where the cylinders tend to shed vortices closer to a certain phase difference. Acoustic resonance actively engages in a constructive interference with the vortex shedding component that can generate positive acoustic energy exchange, which is necessary to sustain the acoustic field in a coupled mechanism of excitation.

Acknowledgements The authors would like to acknowledge the financial support provided by the Natural Sciences and Engineering Research Council of Canada (NSERC).

Declarations

Conflict of interest The authors declare that they have no conflict of interest.

References

Afifi O, Mohany A (2020) Parametric investigation of the flow-sound interaction mechanism for single cylinders in cross-flow. J Pressure Vessel Technol 143(2):021404

Alziadeh M, Mohany A (2018) Near-wake characteristics and acoustic resonance excitation of crimped spirally finned cylinders in cross-flow. J Pressure Vessel Technol 140(5):66

Arafa N, Mohany A (2016) Flow-excited acoustic resonance of isolated cylinders in cross-flow. J Pressure Vessel Technol 138(1):011302

Bai XD, Zhang W, Wang Y (2020) Deflected oscillatory wake pattern behind two side-by-side circular cylinders. Ocean Eng 197:106847

Blevins R (1985) The effect of sound on vortex shedding from cylinders. J Fluid Mech 161:217–237

Blevins R, Bressler M (1993) Experiments on acoustic resonance in heat exchanger tube bundles. J Sound Vib 164(3):503–533

Cantwell B, Coles D (1983) An experimental study of entrainment and transport in the turbulent near wake of a circular cylinder. J Fluid Mech 136:321–374

Clark ST, Besem FM, Kielb RE, Thomas JP (2015) Developing a reduced-order model of nonsynchronous vibration in turbomachinery using proper-orthogonal decomposition methods. J Eng Gas Turbines Power 137(5):66

DeBoo G, Ramsden K, Gesior R, Strub B (2007) Identification of quad cities main steam line acoustic sources and vibration reduction. ASME Pressure Vessels Pip Conf 42827:485–491

Dequand S, Willems J, Leroux M, Vullings R, Van Weert M, Thieulot C, Hirschberg A (2003) Simplified models of flue instruments: influence of mouth geometry on the sound source. J Acoust Soc Am 113(3):1724–1735

Fiquet AL, Vercoutter A, Buffaz N, Aubert S, Brandstetter C (2020) Acoustic resonance in an axial multistage compressor leading to non-synchronous blade vibration. In: ASME Turbo Expo 2020: turbomachinery technical conference and exposition. American Society of Mechanical Engineers Digital Collection

Hambric S, Mulcahy T, Shah V, Scarbrough T, Wu J (2006) Acoustic loading on BWR steam dryers caused by valve singing. In: 9th NRC/ASME symposium on valves, pumps, and inservice testing. Washington, DC, pp 17–19

Hanson R, Mohany A, Ziada S (2009) Flow-excited acoustic resonance of two side-by-side cylinders in cross-flow. J Fluids Struct 25(1):80–94

Hong Z, Wang X, Jing X, Sun X (2020) Frequency lock-in mechanism in flow-induced acoustic resonance of a cylinder in a flow duct. J Fluid Mech 884:66

Ishigai S, Nishikawa E, Nishimura K, Cho K (1972) Experimental study on structure of gas flow in tube banks with tube axes normal to flow: Part 1, karman vortex flow from two tubes at various spacings. Bull JSME 15(86):949–956

Islam M, Mohany A (2020) Vortex shedding characteristics in the wake of circular finned cylinders. Phys Fluids 32(4):045113

Jeong JH (2017) Analysis of vortical flow field related to aero-acoustic sound in an air conditioning system by wall pressure measurement and cfd (2 nd report, blade passing frequency in a blower). J Mech Sci Technol 31(5):2365–2371

Lato T, Mohany A (2019) Passive damping of pressure pulsations in pipelines using Herschel–Quincke tubes. J Sound Vib 448:160–177

Lee PY, Lu WT, Chou ST, Kuo CH (2012) Lock-on characteristics behind two side-by-side cylinders of diameter ratio two at small gap ratio. Exp Fluids 53(4):891–908

Mohany A, Ziada S (2005) Flow-excited acoustic resonance of two tandem cylinders in cross-flow. J Fluids Struct 21(1):103–119

Mohany A, Ziada S (2009a) Effect of acoustic resonance on the dynamic lift forces acting on two tandem cylinders in cross-flow. J Fluids Struct 25(3):461–478

Mohany A, Ziada S (2009b) Numerical simulation of the flow-sound interaction mechanisms of a single and two-tandem cylinders in cross-flow. J Pressure Vessel Technol 131(3):031306

Mohany A, Arthurs D, Bolduc M, Hassan M, Ziada S (2014) Numerical and experimental investigation of flow-acoustic resonance of side-by-side cylinders in a duct. J Fluids Struct 48:316–331

Norberg C (1998) Ldv-measurements in the near wake of a circular cylinder. ASME Paper No FEDSM98-521

Norberg C (2003) Fluctuating lift on a circular cylinder: review and new measurements. J Fluids Struct 17(1):57–96

Oengören A, Ziada S (1998) An in-depth study of vortex shedding, acoustic resonance and turbulent forces in normal triangle tube arrays. J Fluids Struct 12:717–758

Rashwan SS, Mohany A, Dincer I (2020) Investigation of self-induced thermoacoustic instabilities in gas turbine combustors. Energy 190:116362

Rockwood M, Medina A (2020) Controlled generation of periodic vortical gusts by the rotational oscillation of a circular cylinder and attached plate. Exp Fluids 61(2):1–13

Sciacchitano A, Wieneke B (2016) Piv uncertainty propagation. Meas Sci Technol 27(8):084006

Semrau S, Skoda R, Wustmann W, Habr K (2019) Experimental and numerical investigation of noise generation due to acoustic resonance in a cavitating valve. J Sound Vib 463:114956

Shaaban M, Mohany A (2015) Passive control of flow-excited acoustic resonance in rectangular cavities using upstream mounted blocks. Exp Fluids 56(4):1–12

Shaaban M, Mohany A (2019a) Characteristics of acoustic resonance excitation by flow around inline cylinders. J Pressure Vessel Technol 141(5):66

Shaaban M, Mohany A (2019b) Phase-resolved piv measurements of flow over three unevenly spaced cylinders and its coupling with acoustic resonance. Exp Fluids 60(4):71

Shaaban M, Mohany A (2020) Experimental study of the self-excited resonance effect on the dynamic lift and flow structure around inline cylinders. J Fluids Struct 96:66

Shapiro AH (1953) The dynamics and thermodynamics of compressible fluid flow. Ronald Press, New York

Stoica P, Moses RL (2005) Spectral analysis of signals. Pearson Prentice Hall, Upper Saddle River

Sumner D, Wong S, Price S, Paidoussis M (1999) Fluid behaviour of side-by-side circular cylinders in steady cross-flow. J Fluids Struct 13(3):309–338

Trip R, Fransson JH (2017) Bluff body boundary-layer modification and its effect on the near-wake topology. Phys Fluids 29(9):095105

Uchiyama Y, Morita R (2017) Flow-induced acoustic resonance in a closed side branch under a low-pressure wet steam flow. J Pressure Vessel Technol 139(3):66

Van Oudheusden B, Scarano F, Van Hinsberg N, Watt D (2005) Phase-resolved characterization of vortex shedding in the near wake of a square-section cylinder at incidence. Exp Fluids 39(1):86–98

Vitkovicova R, Yokoi Y, Hyhlik T (2020) Identification of structures and mechanisms in a flow field by pod analysis for input data obtained from visualization and piv. Exp Fluids 61(8):1–21

Wadcock PBA (1973) The interference between a pair of circular cylinders normal to a stream. J Fluid Mech 61:499

Wang P, Liu Y (2019) Intensified flow dynamics by second-order acoustic standing-wave mode: vortex-excited acoustic resonances in channel branches. Phys Fluids 31(3):035105

Xu J, Lei J, Wu J, Zhang K (2017) The three-dimensional characteristics of the unsteady wall-pressure in a low-Mach-number rectangular cavity flow with Rossiter model oscillation. Exp Fluids 58(9):1–15

Zdravkovich M, Nuttall J (1974) On the elimination of aerodynamic noise in a staggered tube bank. J Sound Vib 34(2):173–177

Zhou Y (2003) Vortical structures behind three side-by-side cylinders. Exp Fluids 34(1):68–76

Ziada S (2010) Flow-excited acoustic resonance in industry. J Pressure Vessel Technol 132(1):015001

Ziada S, Oengören A, Bühlmann E (1989a) On acoustical resonance in tube arrays part i: experiments. J Fluids Struct 3(3):293–314

Ziada S, Oengören A, Buhlmann ET (1989b) On acoustical resonance in tube arrays part II: damping criteria. J Fluids Struct 3(3):315–324

Publisher's Note Springer Nature remains neutral with regard to jurisdictional claims in published maps and institutional affiliations.